

A NOVEL ANALYSIS ON THE IMPACT OF INTERPRETABLE RADIOMICS APPROACH FOR FOCAL LIVER LESIONS DETECTION IN CONTRAST-ENHANCED ULTRASOUND IMAGES

Abstract

Contrast-enhanced ultrasound (CEUS) imaging has emerged as a valuable tool for detecting focal liver lesions (FLLs). However, accurately characterizing these lesions remains a challenge due to their diverse appearances and complex nature. Radiomics, a promising field that extracts quantitative features from medical images, has shown the potential in improving diagnostic accuracy. In this research paper, we propose a novel analysis of the impact of an interpretable radiomics approach for FLL detection in CEUS images. This research introduces a framework, named feature fusion, comprising three main components: hand-crafted feature extraction, deep feature extraction, a feature fusion unit, and a classifier for generating the final prophecy. The proposed model utilizes a set of twenty frames extracted from CEUS cine clips captured in a CEUS video as a case study. Two different feature types are then extracted. A categorization of merging of all features to generate the ultimate diagnosis. The trials showed that, when compared against a number of cutting-edge models, our strategy performed the best. Additionally, the suggested fused feature offers better interpretability when compared to general CNNs.

Keywords: Contrast-enhanced ultrasound, focal liver lesions, radiomics, interpretable analysis, machine learning, diagnostic accuracy

Authors

T. Haripriya

Research Scholar
School of computing Sciences
VISTAS, Chennai, India
hariswt9@gmail.com

Dr. K. Dharmarajan

Associate Professor
School of computing Sciences
VISTAS, Chennai, India
Dharmak07@gmail.com

I. INTRODUCTION

The second most common reason for cancer-related deaths in the world is HEPATOCELLULAR carcinoma (HCC), the fifth most frequent cancer type [1]. HCC is distinct from other cancers in that it can be identified in patients who have a high risk of acquiring it based just on imaging without requiring histologic confirmation. Dropout in a portal region or delayed phase pictures and arterial stage hyper enhancement are non-invasive diagnostic criteria that have been defined by major guidelines [2]. These are thought to be connected to hemodynamic alterations that happen during hepatocarcinogenesis [4]. In order to diagnose HCC, it is crucial to acquire and analyse polyphase images of dynamically contrast-enhanced computed tomography (CT) or magnetic resonance imaging (MRI). Contrast-enhanced ultrasonography (CEUS) has emerged as a viable imaging technique for evaluating focal liver lesions (FLLs), from prognostic assessment to differential diagnosis and early screening [1–3]. The biggest advantage of CEUS over traditional B-mode ultrasound (BUS) along with additional imaging methods (such as contrast-enhanced MRI and CT) is the ability to view the blood flow improvement distinction among lesions and their surrounding tissue that is healthy in real-time [5]. This is accomplished by injecting microbubble contrast substances (CA), which have a size alike to that of red blood cells [6] and which amplify and inhibit certain reflection echoes from microvessels. In general, a CEUS cine loop is a series of consecutive frames that captures the entire perfusion procedure, including the washing in and washing out of contrast chemicals. Different enhancement patterns linked to tumour angiogenesis have been employed clinically as the main imaging indicators for the evaluation of FLLs [7].

However, accurately characterizing these lesions remains a challenge due to their diverse appearances and complex nature. Radiomics, a burgeoning field in medical imaging, holds great promise in improving diagnostic accuracy by extracting quantitative features from images. In this article, we present a novel analysis of the impact of an interpretable radiomics approach for FLL detection in CEUS images. Our study aims to investigate the effectiveness of radiomics features and their interpretability in the detection of liver lesions precisely.

II. RELATED WORKS

1. Diagnosis of Liver Lesion with Computer Aid: Some research [8] has employed a single technique for segmenting and identifying lesions in computer-assisted diagnoses, such as segmentation based on CT imaging [9]-[11], lesions identification, and lung nodules detection [12]. On the other hand, deep CNN and handmade features have been utilised to segment and detect organ lesions in multi-modal medical scans. To detect FLLs using portal phase CT images, a number of classifications based on deep-learning and recognition techniques must be established [9–15]. Response Evaluation Criteria in Solid Tumours (RECIST) is a system built using a cutting-edge using retinal object scanner (RetinaNet [15]), an anchor optimisation technique, and dense segmentation masks approximating weaker labels. However, the DeepLesion [16] data set, which does not pose a problem with the precise handling of multiphase data, was used to evaluate their approach.

Some studies [15–17] suggested employing assembled convolutional layers and RNN forextraction of inter-phase features to detect FLLs from beginning to end with multiphase CT. A grouped single-shot multi-box detector (GSSD) is suggested in [15] by combining a grouped convolution with explicit decoupling feature extraction. Different neural architectures have effectively adapted to this technique [17].

From the standpoint of the model architecture, it does not solve the misalignment between modalities. The current methods [14–16] presuppose complete intermodal alignment and rely on an established registration methodology, pre processing [17]. The efficacy of the predictive algorithm is because they don't give robustness against misalignments, assurances cannot be made for data with a questionable registration quality. As far as we are aware, our study is the first to provide an end-to-end, DL-based FLL identification from a sizable, unlisted CT database that is multiphase and big.

- 2. Mechanism for Attention:** Deep learning research has recently made the notion of attention a central tenet [14], and the technique has been incorporated into a variety of tasks [13]. The attention mechanism for medical pictures offers a trainable module that dynamically chooses prominent characteristics available in an image that are efficient for given tasks [12–15]. With the help of a feature from a different scale, a soft-attention gating module from [12] creates an attentive zone in the current feature. This module is coupled with Sononet [16] for image categorization and U-net [17] for segmentation of images [18] and Sononet [22] for image classification.

The attention mechanism has been employed in prior studies on medical pictures to make certain that the neural network stays on the objective area (such as a lesion or innards) in a one-phase image. The salient characteristics from multiphase images are exploited in this study using the attention mechanism, which also causes the model to control cross-modal feature aggregation and learning-based transition alignment for task identification.

- 3. Multimodal Registration:** For a computer-aided diagnosis system to be accurate and reliable, medical picture registration is essential. To determine the most effective change between a pair of photos, a number of methods, including statistical [19–21] and learning-based techniques [12–15], have been put forth. In contrast, the polyphase registered job that we provided the model is implicit in the deep space of features, not the picture space.

Only a few techniques have recently been put out for segmenting multifaceted PET-CT scans showing liver abnormalities. The following is a summary of the key multimodal co-learning techniques currently in use: After obtaining features from each modality, modality-specific characteristics are combined [18]–[20] using CNN architecture or conventional techniques [15]. Current deep learning techniques utilise distinct architectures for the encoders for each modality to generate likelihood maps from the many modalities. Traditional approaches use local energies for feature extraction, merging features, and wavelet- and transform-based approaches for feature decomposition, as well as weighted region variance [15]. However, the current multimodal feature extraction techniques all share a fundamental flaw. The highest planes that produce probability maps of CT are the only ones that help the CT encoder blocks.

Neither the registration-focused loss function nor the reference phase data are explicitly provided to the model by this investigation. The dataset has an implicit task that forces the model to optimise object detection efficiency, dynamically focus on the mismatched data, and adjust the deep feature map's outliers.

- 4. Radiomics and FLL Detection:** Radiomics involves the extraction of a large number of quantitative features from medical images, which can be analyzed using machine learning algorithms to derive meaningful insights. By applying radiomics to CEUS images, researchers have attempted to identify and quantify distinct features that can differentiate between benign and malignant liver lesions. These features include intensity-based measures, shape descriptors, and texture features, which capture various aspects of lesion characteristics.

The interpretability of radiomics is a critical aspect of medical imaging analysis. While machine learning algorithms provide powerful predictive models, the lack of interpretability can hinder the adoption of radiomics in clinical practice. Researchers have recognized the need for interpretable radiomics approaches that provide insights into the features driving diagnostic decisions. Techniques such as feature importance analysis, heatmaps, decision trees, and radiomics signatures have been employed to enhance the interpretability of radiomics models.

- 5. Problem Statement:** Focal liver lesions (FLLs) are a communal finding in clinical practice, and accurate detection and characterization of these lesions are essential for effective patient management. While contrast-enhanced ultrasound (CEUS) imaging has shown potential in FLL detection, the subjective interpretation of CEUS images presents challenges in achieving consistent and reliable results. Furthermore, the complex nature of FLLs necessitates a comprehensive analysis of radiomics features to improve diagnostic accuracy. Therefore, the problem at hand is to investigate the impact of an interpretable radiomics approach in enhancing FLL detection in contrast-enhanced ultrasound images, aiming to develop a more objective and reliable diagnostic method for better patient outcomes.

III. MATERIALS AND METHODS

- 1. Proposed Architecture:** We give an overview of the suggested feature fusion framework. Fig. 1 depicts the suggested framework, which consists of three main parts: the Feature extraction methods include hand-crafted feature extraction, deep feature extraction, feature fusion, and classifiers that produce the final prediction. 20 frames from a CEUS video obtained through the cine clips of CEUS are used as a case in this model. Two different feature types are then extracted. Classifier uses the fusion of all features to create the final diagnosis.

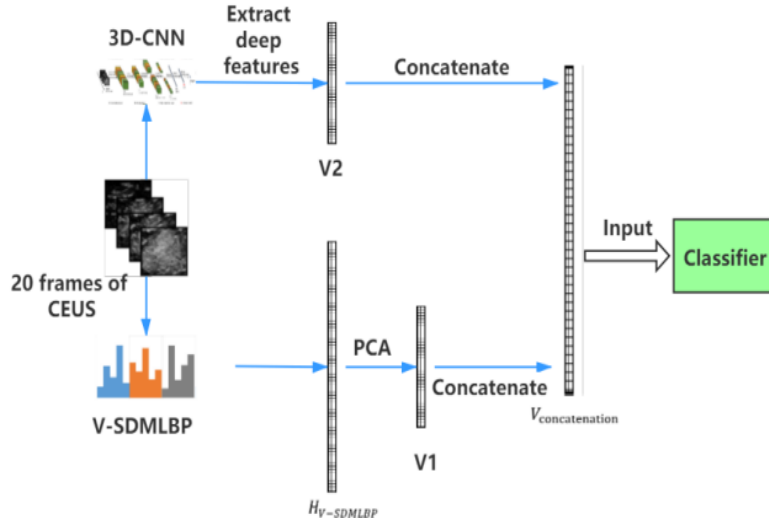


Figure 1: The overall layout of the suggested algorithm [17].

RIU2 has improved, and LBP is now defined as:

$$LBP^{RIU2} = \begin{cases} \sum_{i=0}^{p-1} s(g_p - g_c) \text{ if } U(LBP) \leq 2 \\ p + 1 \text{ otherwise} \end{cases} \quad (1)$$

$$S(x) = \begin{cases} 1, x \geq 0 \\ 0, x < 0 \end{cases} \quad (2)$$

Where GC stands for the central pixel, g_p for the neighbouring pixels, I for the pixel location, P for the number of neighbouring pixels, and $U(\cdot)$ for the mode of conformal mapping. In binary coding, the relationships among neighbouring pixels are encrypted. DMLBP and SMLBP are utilised to seizure differences and likeness matches of enhanced dispersal in order to acquire the higher-level features found in ultrasound pictures. Main, 4 types of identically are described.

$$n_{1-1} = \sum_{i=0}^{p-1} a(i)b(i) \quad (3)$$

$$n_{1-0} = \sum_{i=0}^{p-1} a(i)[1 - b(i)] \quad (4)$$

$$n_{0-1} = \sum_{i=0}^{p-1} [1 - a(i)]b(i) \quad (5)$$

$$n_{0-0} = \sum_{i=0}^{p-1} [1 - a(i)][1 - b(i)] \quad (6)$$

where LBP codes a and b are 2. Second, the values of SMLBP and DMLBP are determined for each pixel as follows:

$$\text{SMLBP} = \sum_{i=0}^{p-1} s(s_i - m_s) \times 2^i \quad (7)$$

$$\text{DMLBP} = \sum_{i=0}^{p-1} s(d_i - m_d) \times 2^i \quad (8)$$

$$s_i = \frac{n_{1-1}}{n_{1-1} + n_{0-0} + \varepsilon} \quad (9)$$

$$s_i = \frac{n_{1-0}}{n_{1-0} + n_{0-1} + \varepsilon} \quad (10)$$

where p is the neighbouring sample pixel number, s_i is the resemblance identical ration, d_i are the difference identical ration, m_s and m_d are averages of s_i and d_i , and i is the pixel order.

2. **Feature Extraction:** Due to its capability to automatically acquire higher-level characteristics, CNN has shown to be extremely powerful in CAD systems [20]. It can excerpt previously unknown discrimination features. The temporal features included in sequential images are ignored by 2D-CNN, which can solitary handle the 3-D feature in a single frame. So, for more advanced spatial-temporal information as of CEUS, we use a 3D-CNN.
3. **Data Preparation:** One video is used to build a sample 20-frame picture list. The radiologists manually marked and reduced the tumour in the final LP frame because LP frames tend to have constant elevated intensity. Because the patients remained nearly motionless, the identical Region of Interest identified in the LP frame could be cut from all frames in a CEUS film. Cropped photos were downsized to a 100100 size for hand-crafted feature extraction. While they were reduced in size to 3232 for deep feature extraction to speed up processing.

By separating and expanding the basic dataset using several procedures, we created two distinct datasets. To create the dataset 1 for model optimisation, we directly augment the first dataset. There were two steps in the data augmentation procedure. The first step is to resample the basic CEUS videos by shifting the mining location at every interlude. Thus, many picture lists could be produced from a single CEUS video. We comparatively oversampled the atypical HCC videos since the FNH instances outnumber atypical HCC cases. Then, 201 FNH cases and 216 HCC cases were added to our database. Step two: instead of rotating or cropping the photos, we randomly altered the brightness and contrast ratio to prevent the tumor's shape from changing. Then, we acquired an expanded dataset that included 1961 HCC cases and 1811 FNH cases. For model evaluation, we put up dataset 2. First, we chose 30 cases—15 of FNH and 15 of atypical HCC—at random from the initial dataset to serve as the test set. Through the two stages described above, the rest of the dataset was expanded to serve as the training set.

4. **Performance Analysis:** Differentially divided dataset, we evaluated the "fused feature + SVM" architecture five times. The training set was expanded for each epoch, and 30 initial independent examples were used for assessment. Three frames from one phase of the CEUS data were used by the author [21] to analyse features using Deep Canonical

A NOVEL ANALYSIS ON THE IMPACT OF INTERPRETABLE RADIOMICS APPROACH FOR FOCAL LIVER LESIONS DETECTION IN CONTRAST-ENHANCED ULTRASOUND IMAGES

Correlation Analysis (DCCA). The multi-view features were then given to a multiple kernel learning classifier for classification. These algorithms were refined using a unique dataset.

IV. RESULTS AND ANALYSIS

- 1. Model Optimisation Outcomes:** Table I displays the median and range of the evaluation measures for KNN, MLP, and SVM. These three classifiers all showed strong performance. Better and roughly equal mean classification performance was obtained by the SVM and MLP. The identical performance of these three classifiers demonstrates the robustness and representation of the fused feature.

Table 1: Classifiers' performance (Unit: %) [17].

Classifier	Accuracy	Precision	F1-scores	Sensitivity	Specificity
KNN	97.75 ± 0.82	98.50 ± 0.50	97.81 ± 0.80	97.15 ± 1.32	98.40 ± 0.55
MLP	98.11 ± 1.97	99.02 ± 1.10	98.04 ± 2.03	97.19 ± 4.05	99.01 ± 1.13
SVM	98.35 ± 0.56	97.87 ± 1.11	98.84 ± 0.80	98.82 ± 0.79	98.34 ± 0.57

Table 2: The experiment's results in ablation (unit:%)

Approach	Sensitivity	Specificity	Accuracy
Hand-crafted+SVM	94.79	93.59	94.88
3D-CNN attention	94.58	94.63	95.78
Deep+SVM	95.42	99.23	97.56
Fused+MLP	97.87	99.35	98.11
Fused+SVM	97.98	98.99	98.89

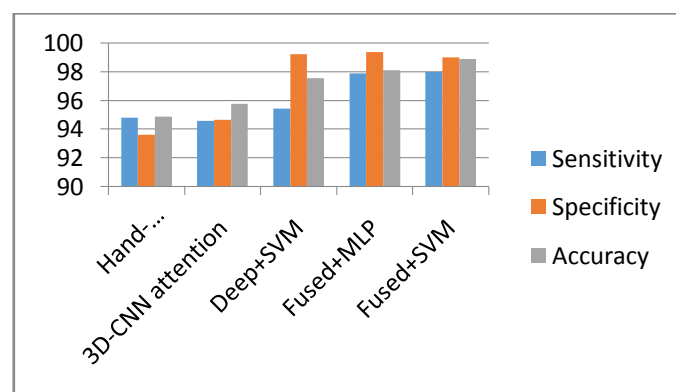


Figure 2: Graphical representation of Performance analysis

2. **Results of the Tests with Ablation:** Table II displays the findings from ablation trials. 'Deep+SVM' outperforms 'Hand-crafted+SVM' by 3.32%, proving the depth features' superiority over the hand-crafted features. These three comparisons demonstrate the effectiveness of feature fusion: 'Fused+MLP' outperforms '3D-CNN_attention' with a 3.77% advantage; 'Fused+SVM' outperforms 'Deep+SVM' with a 1.33% advantage; and 'Hand-crafted+SVM' with a 4.01% advantage, as shown in fig. 4.
3. **The Outcome of Deep Features Visualization:** In Figs. 2 and 3, we deliberately sketched up the tumour boundary in red ink to further illustrate the visualisation of the features. Because figure (a) in Figures 2 and 3 is not sufficiently increased, we were unable to line their boundary up. Prototype HCC and FNH heat maps without spoke wheels augmentation patterns are shown in Figs. 2 and 3, respectively. Two features can be seen. First, the localised liver lesions are the focal point of hotspots in every frame, demonstrating the 3D-CNN's ability to record discriminative regions. Second, there are a lot more hotspots in the PVP and LP photos than in the AP. This implies that 3D-CNN emphasises PVP and LP more, which is chronologically compatible [7, 8].
4. **Performance Evaluation Findings:** Among these cutting-edge techniques for FLL diagnosis, our suggested algorithm performed the best. Single-frame training and evaluation are done with VGG16 [22].

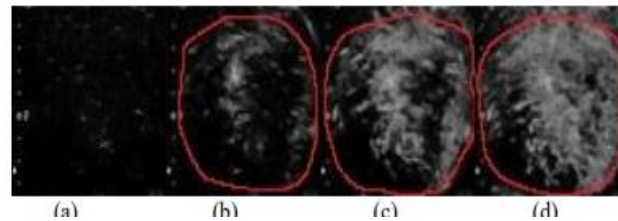


Figure 3: The heat maps of a CEUS-framed instance of atypical HCC [17].

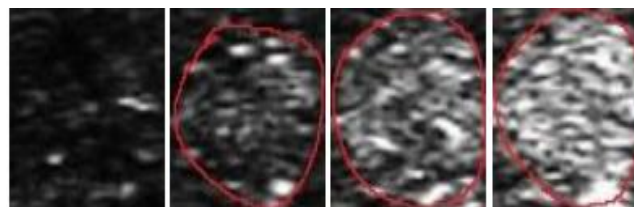


Figure 4: FNH case's heatmaps sans a spoke-wheel augmentation pattern [17].

V. DISCUSSION

Radiologists can find precise diagnosis semantics with the aid of the discriminative areas of the deep features. Then, we combined extensive features alongside the previously suggested manually created spatial-temporal characteristics to achieve performance that was superior to both of them. It is important to note that by using the fused feature, several different types of classifiers achieved good performance. The diversity of classifiers could show how reliable the fused feature is. PCA damages the comprehensibility of the fused features by erasing the original hand-crafted features. Fortunately, the covariance matrix's

size of eigenvalues reflects the weight of various patterns, making it easier to identify the most important patterns.

VI. CONCLUSION

As a result, we suggest a computer-aided diagnosis system that combines hand-crafted and deep features to effectively differentiate atypical hepatocellular carcinoma and focal nodular hyperplasia. The features of deep convolution are obtained using a pre-trained 3D-CNN model, while a cutting-edge hand-crafted technique is used to extract the features of hand-crafted. These features are then merged and inputted into a classifier for accurate diagnosis. The fusion of features demonstrates strong performance across various classifiers, highlighting its robustness. Comparatively, the fused feature model outperforms both the hand-crafted features and the standalone 3D-CNN model, offering not only improved performance but also enhanced interpretability. As a result, our algorithm holds significant potential for clinical applications in atypical HCC diagnosis, alleviating patients' suffering and reducing the workload for sonographers.

REFERENCES

- [1] S. Mittal and H. B. El-Serag, "Epidemiology of hcc: consider the population," *Journal of clinical gastroenterology*, vol. 47, p. S2, 2013.
- [2] European Association for the Study of the Liver and European Organisation for Research and Treatment of Cancer, "Easl–eortc clinical practice guidelines: Management of hepatocellular carcinoma," *Journal of Hepatology*, vol. 56, no. 4, pp. 908–943, 2012.
- [3] M. Omata et al., "Asia–pacific clinical practice guidelines on the management of hepatocellular carcinoma: a 2017 update," *Hepatology International*, vol. 11, no. 4, pp. 317–370, 2017. IEEE TRANSACTIONS ON EMERGING TOPICS IN COMPUTATIONAL INTELLIGENCE 10
- [4] J. K. Heimbach et al., "Aasld guidelines for the treatment of hepatocellular carcinoma," *Hepatology*, vol. 67, no. 1, pp. 358–380, 2018.
- [5] A. Kitao et al., "Hepatocarcinogenesis: multistep changes of drainage vessels at ct during arterial portography and hepatic arteriography—radiologic-pathologic correlation," *Radiology*, vol. 252, no. 2, pp. 605–614, 2009.
- [6] Professional Committee for Prevention and Control of Hepatobiliary and Pancreatic Diseases of Chinese Preventive Medicine Association, et al., "Guideline for stratified screening and surveillance of primary liver cancer (2020 Edition)," *Chinese Journal of Hepatobiliary Surgery*, vol. 27, no. 1, pp. 12–29, 2021, 2021.
- [7] E. Goceri, Z. K. Shah, R. Layman et al., "Quantification of liver fat: A comprehensive review," *Computers in Biology and Medicine*, vol. 71, pp. 174–189, Apr 2016.
- [8] T. A. Morgan, K. E. Maturen, N. Dahiya, et al., "US LI-RADS: ultrasound liver imaging reporting and data system for screening and surveillance of hepatocellular carcinoma," *Abdominal Radiology*, vol. 43, no. 1, pp. 41–55, Jan 2018.
- [9] Y. Kono, A. Lyschik, D. Cosgrove, et al., "Contrast Enhanced Ultrasound (CEUS) Liver Imaging Reporting and Data System (LI-RADS (R)): the official version by the American College of Radiology (ACR)," *Ultraschall in Der Medizin*, vol. 38, no. 1, pp. 85–86, Jan 2017.
- [10] F. Piscaglia, R. Lencioni, E. Sagrini, et al., "CHARACTERIZATION OF FOCAL LIVER LESIONS WITH CONTRAST-ENHANCED ULTRASOUND," *Ultrasound in Medicine and Biology*, vol. 36, no. 4, pp. 531–550, Apr 2010.
- [11] D. Christofides, E. Leen, and M. A. Averkiou, "Evaluation of the Accuracy of Liver Lesion DCEUS Quantification With Respiratory Gating," *IEEE Trans. Med. Imaging*, vol. 35, no. 2, pp. 622–629, 2016.
- [12] S. Bakas, M. Doulgarakis-Kontoudis, G. J. Hunter, P. S. Sidhu, D. Makris, and K. Chatzimichail, "Evaluation of indirect methods for motion compensation in 2-d focal liver lesion contrast-enhanced ultrasound (ceus) imaging," *Ultrasound in Medicine & Biology*, vol. 45, no. 6, pp. 1380–1396, 2019.
- [13] U. Yasuyuki, K. Shohei, K. Masahiro, O. Yona, I. Hideyuki, and U. Katsuhiko, "Correction of liver displacement due to irregular respiration for SPECT images obtained using a multiple short-time

A NOVEL ANALYSIS ON THE IMPACT OF INTERPRETABLE RADIOMICS APPROACH FOR FOCAL LIVER LESIONS DETECTION IN CONTRAST-ENHANCED ULTRASOUND IMAGES

- acquisition with breath-holding technique,” *Radiological physics and technology*, vol. 5, no. 1, pp. 71–77, 2012.
- [14] Z. Ye, I. Huth, D. C. Weber, and A. J. Lomax, “A statistical comparison of motion mitigation performances and robustness of various pencil beam scanned proton systems for liver tumour treatments,” *Radiotherapy and Oncology*, vol. 128, no. 1, pp. 182–188, 2018.
- [15] J. Zhang, M. Ding, F. Meng, M. Yuchi, and X. Zhang, “Respiratory motion correction in free-breathing ultrasound image sequence for quantification of hepatic perfusion,” *Med. Phys.*, vol. 38, pp. 4737–4748, 2011.
- [16] Lee SG, Kim E, Bae JS, Kim JH, Yoon S. Robust end-to-end focal liver lesion detection using unregistered multiphase computed tomography images. *IEEE Transactions on Emerging Topics in Computational Intelligence*. 2021 Dec 15.
- [17] Zhou J, Pan F, Li W, Hu H, Wang W, Huang Q. Feature fusion for diagnosis of atypical hepatocellular carcinoma in contrast-enhanced ultrasound. *IEEE Transactions on Ultrasonics, Ferroelectrics, and Frequency Control*. 2021 Sep 6;69(1):114-23.
- [18] Wan P, Chen F, Shao W, Liu C, Zhang Y, Wen B, Kong W, Zhang D. Irregular respiratory motion compensation for liver contrast-enhanced ultrasound via transport-based motion estimation. *IEEE Transactions on Ultrasonics, Ferroelectrics, and Frequency Control*. 2020 Oct 27;68(4):1117-30.
- [19] Xue Z, Li P, Zhang L, Lu X, Zhu G, Shen P, Shah SA, Bennamoun M. Multi-modal co-learning for liver lesion segmentation on PET-CT images. *IEEE Transactions on Medical Imaging*. 2021 Jun 16;40(12):3531-42.
- [20] Turco S, Tiyyarattanachai T, Ebrahimkheil K, Eisenbrey J, Kamaya A, Mischi M, Lyshchik A, El Kaffas A. Interpretable machine learning for characterization of focal liver lesions by contrast-enhanced ultrasound. *IEEE Transactions on ultrasonics, ferroelectrics, and frequency control*. 2022 Mar 23;69(5):1670-81.
- [21] Guo L, Wang D, Xu H, Qian Y, Wang C, Zheng X, Zhang Q, Shi J. CEUS-based classification of liver tumors with deep canonical correlation analysis and multi-kernel learning. In *2017 39th Annual International Conference of the IEEE Engineering in Medicine and Biology Society (EMBC) 2017 Jul 11 (pp. 1748-1751)*. IEEE.
- [22] Simonyan K, Zisserman A. Very deep convolutional networks for large-scale image recognition. *arXiv preprint arXiv:1409.1556*. 2014 Sep 4.